

We are IntechOpen, the world's leading publisher of Open Access books Built by scientists, for scientists

6,900

Open access books available

185,000

International authors and editors

200M

Downloads

Our authors are among the

154

Countries delivered to

TOP 1%

most cited scientists

12.2%

Contributors from top 500 universities



WEB OF SCIENCE™

Selection of our books indexed in the Book Citation Index
in Web of Science™ Core Collection (BKCI)

Interested in publishing with us?
Contact book.department@intechopen.com

Numbers displayed above are based on latest data collected.
For more information visit www.intechopen.com



The Fracture Behavior of Pure and Hybrid Intraply Knitted Fabric-Reinforced Polymer Composites

Huseyin Ersen Balcioglu and Hayri Baytan Ozmen

Abstract

Due to the high synergistic effects of the components, hybrid composite materials are more advantageous than nonhybrid composite materials for advanced engineering applications. Additionally, knitted fabrics may have a different behavior than woven ones. Although the nonhybrid composites have only one reinforcing fiber type, the hybrid composites have multiple reinforcing fibers. In this chapter, fracture characterizations of laminated composites reinforced with intraply pure and hybrid knitted fabrics are experimentally and numerically investigated under different loading conditions. For this purpose, pure (100%) and hybrid fabrics (50–50%), which have 1×1 rib-knitted structure, were knitted by using glass and carbon fibers. Also, hybrid fabrics were knitted in three different widths in order to investigate the effect of knitting pattern width on the fracture toughness. Fracture toughness and energy strain release rates of pure and hybrid Arcan test specimens were determined under mode I (0°), mixed-mode I/II (30° , 45° , and 60°), and mode II (90°) loading conditions. Also, the J-integral method was used to determine the fracture toughness. Experimental and numerical results were found to be consistent. When the results obtained from pure and hybrid fabrics are compared, it is seen that hybridization had positive effects on the fracture strength of composite material compared to pure glass/epoxy material. Additionally, as the width of the pattern decreased, the fracture strength of the hybrid composites increased. In this respect, the hybridization processing should be done in the narrowest pattern width for higher resistance to fracture.

Keywords: fracture toughness, strain energy release rate, Arcan fracture test, pure and hybrid laminated composite, knitted fabric, J-integral method

1. Introduction

High strength to low weight ratio is a sought-after feature in the materials used in the structural elements of today's world. With the technological advances in recent years, composite materials are used in many industries, where durability and lightness are at the forefront, especially from the aerospace to automotive sectors. Polymeric composites have been used in many engineering applications due to their high strength in proportion to their weight, high stability, rigidity, superior corrosion, and fatigue resistance [1–3]. Woven or knitted fabrics of durable synthetic fibers such as glass, carbon, or aramid are used to reinforce polymer matrix

composite. Woven reinforcement exhibits good stability in the warp and weft directions and offers the highest cover or yarn packing density in relation to fabric thickness [4]. Knitting is another technique of fabric formation for reinforcing. The fabric is formed by the inter-looping of yarn. The inter-looping of yarn can be done in two ways, namely, warp and weft knitting [5]. Complex lattice structures can be produced by local deformation of the loop in knitted structures. The loop that oriented through-thickness direction improves the out-of-plane mechanical properties of the structure. In addition, thanks to the perfectible geometry of the loop, high impact resistance and damage tolerance can be achieved. Textile-reinforced composites consist of a textile form as the reinforcement phase and usually a polymer for the matrix phase. 2D or 3D woven fabrics, knitted fabrics, stitched fabrics, braids, nonwovens, and multiaxial fabrics can be used as textile materials. Each of these textile forms has its own fiber architecture and combination of properties such as strength, stiffness, flexibility, and toughness, which are reflected on the composite performance to a certain extent [6]. A number of researchers have studied the damage strength of knitted fabric-reinforced composite structures under loading of tensile, compressive, fracture, and impact [7–10].

Lower cost, lower density, comparable specific strength, and better deformation capacity are the advantages of glass fibers as compared to carbon fibers. However, types of glass fibers have worse mechanical properties than carbon fibers, which is a limitation to the applications, especially when these materials are exposed to more severe stresses. One way to overcome this problem is hybridization, i.e., the combination of glass and carbon fibers, using a matrix compatible with both fibers, to obtain a composite material with satisfactory properties and lower cost. Hybridization with different fiber types within laminated composites increases the design space and opens up possible new engineering applications with optimized mechanical and functional properties. In addition, in the classical composites, the hybridization of carbon and glass fibers may cause a positive hybrid effect, which relies on the increase of carbon fibers failure strain, when compared to the pure carbon-based composites [11]. Generally, as far as the strength of the carbon/glass hybrid is concerned, the higher the volume percentage of carbon fibers is, the stronger the hybrid laminate becomes. The reason is that the carbon fibers are very tough and stiff, while the glass fibers are less stiff and less durable. In carbon/glass fiber-reinforced composites, an advantageous hybrid effect is also observed, which consists in increasing the carbon fiber failure strain when compared to the pure carbon fiber. In the literature, there are studies investigating the effects of carbon/glass hybridization on mechanical behavior. Tabrizi et al. [12] have investigated damage evolution in carbon/glass fiber hybrid composites with various stacking sequences under pure bending and tensile loading conditions. Swolfs et al. [13] concluded that the effect for tensile failure strain is well established, with a typical range of 10–50% for traditional hybrid composites such as carbon/glass. Wisnon et al. [14] have investigated hybrid effects on thin ply carbon/glass unidirectional laminates. Test results showed that the magnitude of the hybrid effect depends on the ply thickness. Dong and Davies [15] have studied the mechanical properties of the hybrid composites reinforced with the glass and carbon fibers. Naito and Oguma [16] have investigated tensile properties and fracture behavior of carbon/glass hybrid thermoplastic composite rods consisting of unidirectional PAN-based carbon fiber, braids of E-glass glass fibers, and thermoplastic epoxy matrix.

Composite materials used for structural purposes can be damaged during manufacturing, assembly, and usage of them. These damages can cause breaking of the materials under environmental effects and external loadings. One of these damages is crack onset and fracture, which depends on crack formation. Fracture, which is precarious for composite structures, can cause loss of life and property. Thus, the fracture analysis of the composite materials, especially focusing on the

growth of defects that occur during the service that leads to destruction, is vital to the safety of the composite structures. The value of fracture toughness of composite materials strongly depends on three loading states at the end of the crack tip as the tensile opening mode (mode I), the in-plane shear mode (mode II), and the out-of-plane shear mode (mode III). However, fracture state does not form in pure mode I or mode II in the fiber-reinforced composite materials due to combined loading or anisotropy of composite structures [17]. For this reason, the study of the mixed-mode interlaminar fracture toughness is very important. Zhao et al. [18] have studied interlaminar fracture toughness of hybrid woven carbon-Dyneema composites with different hybridization schemes. The results showed that hybridization improves both mode I and mode II fracture toughness of carbon-Dyneema interfaces. Bienias et al. [19] have investigated interlaminar fracture toughness of woven glass and carbon-reinforced multidirectional fiber metal laminates under mixed-mode (mode I/II) loading. Jung and Kim [20] have investigated the fracture toughness of carbon-glass/epoxy interply hybrid composite under mode I loading condition. Saidane et al. [21] have investigated mode-I interlaminar fracture toughness of flax; glass and hybrid flax-glass fiber are woven composites by using a double cantilever beam test method. Swolf et al. [22] have studied translaminar fracture toughness of woven carbon/glass hybrid composites under impact loading.

Hybridizing two or more reinforcement materials within a matrix seeks to enhance the advantages of the reinforcing constituents and lessen the effect of the less desirable characteristics. In this study, the fracture toughness of pure and intraply hybrid knitted fabric-reinforced laminated composite plates have been investigated, experimentally and numerically. For this purposes, hybrid fabrics were knitted in a 1×1 rib-knitted structure by using glass and carbon fibers with equal weight carbon/glass fibers (50–50%). In order to investigate the effect of the knitting pattern width on the fracture behavior, the reinforcing hybrid fabrics were knitted at three different widths, such as 50, 25, and 12.5 mm. Arcan test apparatus was used to define mode I (opening mode), mode II (shearing mode), and mode I/II (mixed-mode) fracture toughness of test specimens. Also, fracture toughness for all composite samples was numerically determined in finite element analysis by using the J-integral method.

2. Materials and methods

2.1 Knitting process of hybrid fabric

Knitting is primarily classified as weft knitting and warp knitting. This classification is based on the direction of movement of yarn with respect to the direction of fabric formation. If the yarns run in the width or crosswise direction with reference to the direction of fabric formation during knitting, then the process of knitting is called weft knitting. The yarns in the knitted structure are just like weft yarns in woven fabrics. The weft-knitted fabrics made with one set of needles arranged in the grooves on one needle bed are called single jersey fabrics or plain knitted fabrics. In the experimental study, intraply hybrid reinforcement fabrics, which have 1×1 rib knitting structure, were knitted in a V-bed semi-automatic knitting machine. For this aim, 2400tex E-glass fibers and 3K carbon fibers were used as a knitting reinforcement element.

A loop is called a face loop or back loop according to the direction of the passing of one loop through another one during inter-looping (**Figure 1a**). A course is a horizontal row of loops produced by all the adjacent needles during the same knitting cycle. A wale is a vertical column of loops made by the same needle in

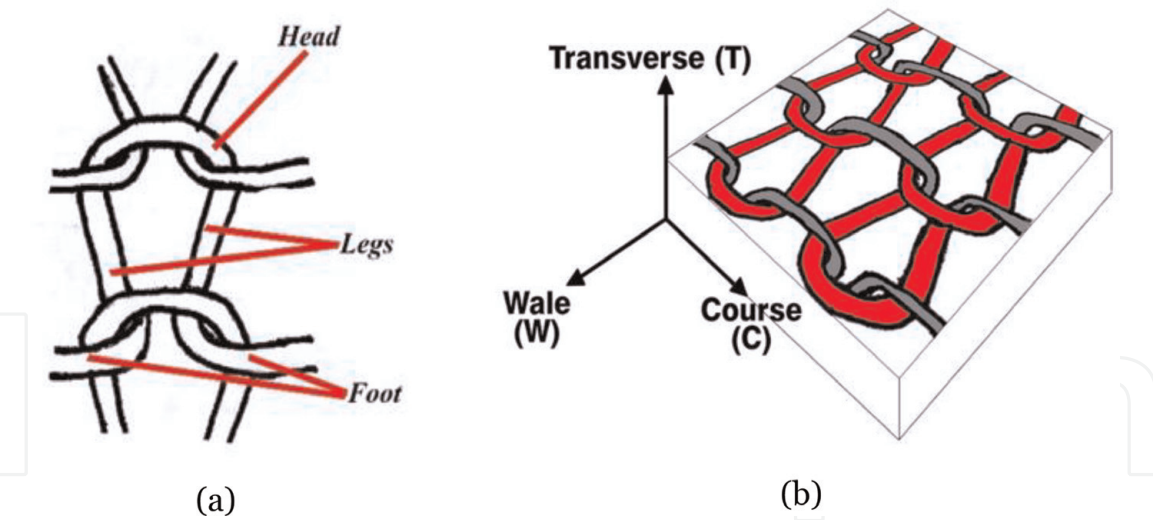


Figure 1.
(a) A knitted loop and (b) wale and course directions of loops.

Fiber type	Pattern width (mm)		
	12.5	25	50
Glass	4	8	15
Carbon	4	9	17

Table 1.
The row numbers of glass and carbon fibers for desired pattern widths.

successive knitting cycles. The direction of course and wale in weft-knitted fabric is shown in **Figure 1b**.

The row numbers of glass and carbon corresponding to the considered width are shown in **Table 1**. The average width of a single row is around 2.8–3.3 mm in the scope of this study. The average weight of hybrid and non-hybrid reinforcement fabrics was 730 g/m². The thickness of knitted fabric is approximately 2.7 mm.

2.2 Manufacturing of hybrid laminated composites

The matrix material was procured from Duratek Epoxy and Polyurethane Systems in Turkey. Hybrid laminated composite materials having four laminas were produced by hand lay-up methods. After all, laminas were saturated with epoxy resin; semi-product laminated composites were cured at 100°C under pressure of 8 MPa for 100 min, by using temperature-time-pressure-controlled hydraulic press.

After this process, the composite plates were cooled to room temperature under the same pressure to avoid warping effects. The fiber volume fractions for hybrid

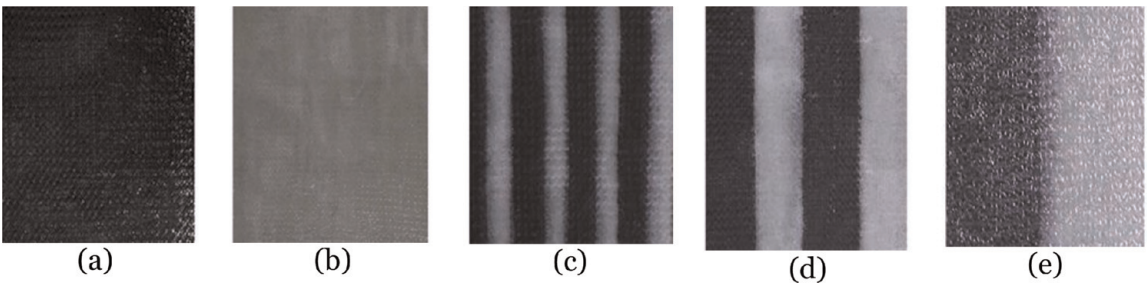


Figure 2.
Manufactured knitted fabric laminated composites (a) pure carbon/epoxy and (b) pure glass/epoxy fabric, and hybrid carbon-glass/epoxy composites with (c) 12.5, (d) 25, and (e) 50 mm pattern widths.

carbon-glass/epoxy laminated composites were determined as 55% approximately. In this study, the hybridization process is carried out using reinforcing fabrics knitted with different types of fibers on the same layer [23–25]. During stacking of layers, the same type of fibers was brought one on the top of another. The photographic representation of produced knitted hybrid composites is shown in **Figure 2**.

3. Experimental study

3.1 Determination of fracture toughness

The fracture toughness of pure and hybrid knitted laminated composites was determined for mode I (0°), mode I–II (30° , 45° , and 60°), and mode II (90°) by using modified Arcan test apparatus. In this context, Arcan test samples were cut with a CNC router machine by using 3 mm cutter blade (**Figure 3**). After cutting, crack having 4 mm was created on the Arcan test sample by using a jigsaw, which had 0.6 mm diameter. Hybrid composite specimens had two different reinforcement materials like glass and carbon fibers in the same layer. Therefore, crack onset in a different reinforcement material may occur in a different shape under load. Crack in the Arcan test sample having the same knitting pattern width was varied in two different forms to investigate crack onset mechanism in glass and carbon fibers.

In the first form, the crack was opened to glass fiber side and made to move toward the carbon fiber side. In the other form, the crack was opened to carbon fiber side and made to move toward the glass fiber side (**Figure 3c, d**). Linear elastic

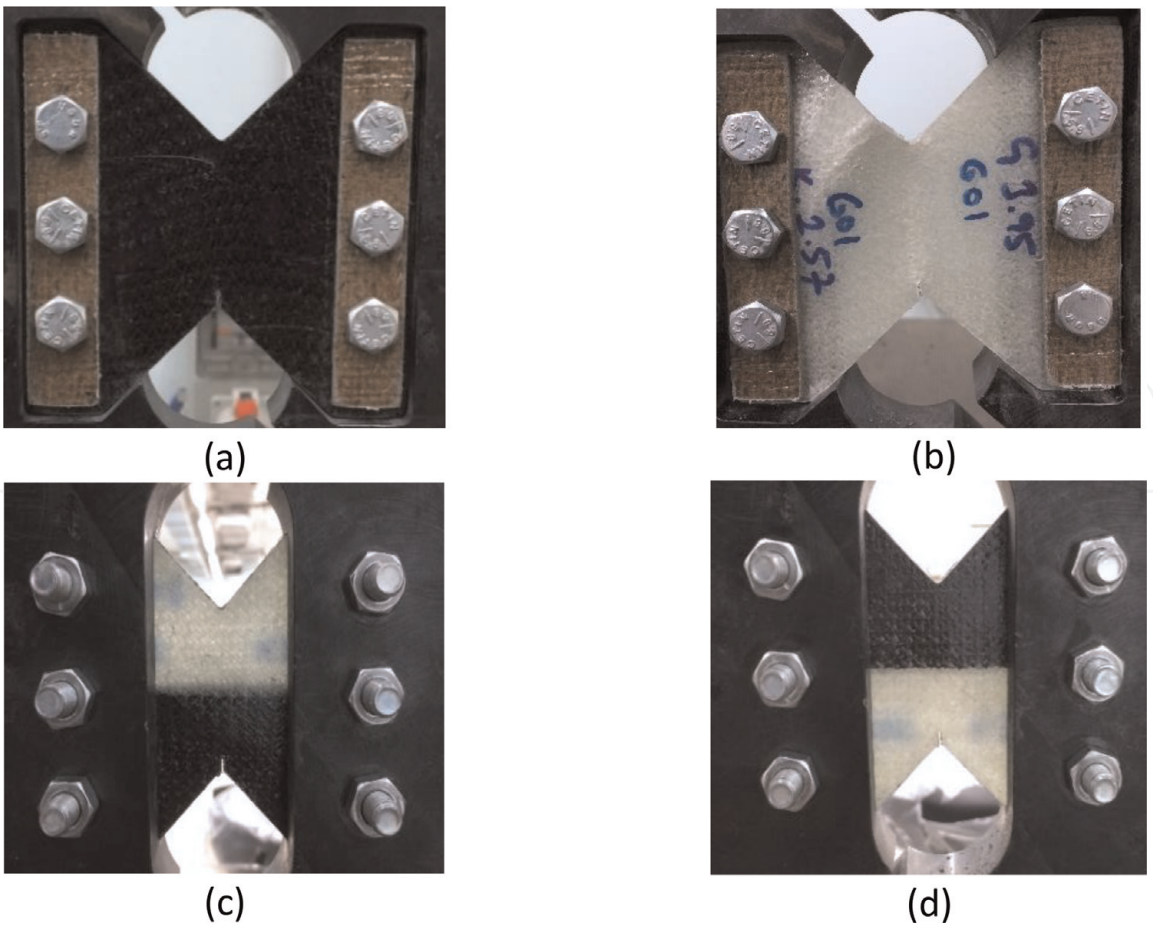


Figure 3.
Arcan test specimen (a) pure carbon/epoxy, (b) pure glass/epoxy, and hybrid carbon-glass/epoxy having (c) carbon side crack and (d) glass side crack.

fracture mechanics (LEFM) has been found as a useful tool for the investigation of cracks in composite materials. The purpose of fracture toughness testing is to determine the value of the critical stress intensity factor or plane strain fracture toughness K_C . The values of fracture toughness for the opening mode (mode I), tension/shearing mode (mixed-mode I/II), and shearing mode (mode II) were found using the following formulas. The stress intensity factor, K_C , at the tip of the crack for the Arcan test tension specimens is given by Eq. (1):

$$K_C = \frac{P_c \sqrt{\pi a}}{wt} f\left(\frac{a}{w}\right) \quad (1)$$

where P_c is the fracture load, a is the crack length, w is specimen width, t is the specimen thickness, and $f\left(\frac{a}{w}\right)$ is a geometrical factor. ASTM D5045 gives some guidance for plane strain fracture toughness and strain energy release rate [26]. ASTM D5045 is a reference in the literature for the studies, which are about the fracture behavior of fiber-reinforced polymer composites [27–29]. K_I (opening mode stress intensity factor) and K_{II} (shearing mode stress intensity factor) state the severity of the crack tip environment, and it is logical to characterize resistance to fracture by a critical value, that is, K_{IC} and K_{IIC} (Eq. 2). When the applied normal stress reaches the failure stress, the stress intensity factors K_I and K_{II} become the critical stress intensity factor (K_{IC} and K_{IIC}), which is taken as the fracture toughness of the composite specimens [30, 31]. The stress intensity factors ahead of the crack tip for Arcan test sample are calculated by using Eq. (2) [32–34]:

$$\begin{array}{ll} \text{Mode I fracture toughness} & \text{Mode II fracture toughness} \\ K_{IC} = \frac{P_{\max} \sqrt{\pi a}}{wt} f_I\left(\frac{a}{w}\right) & K_{IIC} = \frac{P_{\max} \sqrt{\pi a}}{wt} f_{II}\left(\frac{a}{w}\right) \end{array} \quad (2)$$

The geometric factor formulas $f_I\left(\frac{a}{w}\right)$ and $f_{II}\left(\frac{a}{w}\right)$ used to calculate the K_I and K_{II} were provided by Eqs. (3–4) [32]:

$$f_I\left(\frac{a}{w}\right) = 182.12\left(\frac{a}{w}\right)^4 - 293.81\left(\frac{a}{w}\right)^3 + 187.87\left(\frac{a}{w}\right)^2 - 51.492\left(\frac{a}{w}\right) + 6.1137 \quad (3)$$

$$f_{II}\left(\frac{a}{w}\right) = -18.622\left(\frac{a}{w}\right)^4 + 36.753\left(\frac{a}{w}\right)^3 - 25.182\left(\frac{a}{w}\right)^2 + 7.759\left(\frac{a}{w}\right) + 0.0944 \quad (4)$$

For the mixed-mode loading effective fracture toughness, K_{eff} is calculated by Eq. (5) [35, 36]:

$$K_{eff} = \sqrt{K_I^2 + K_{II}^2} \quad (5)$$

where K_I and K_{II} are components of the fracture toughness in mode I and mode II directions. To calculate the values of mode I and mode II and total mixed-mode components of knitted fabric-reinforced composites, the material anisotropy should be taken into account.

3.2 Determination of strain energy release rate

The energy release rate (G) is defined as the amount of energy released per unit of the new fractured area formed due to cracking. The energy release rate is also defined as the crack extension force. A simple procedure using energy concepts is utilized to develop an analytical description of the crack extension force. The energy

release rates for orthotropic material with the crack line parallel to the principal orthotropic direction which coincides with the fiber orientation can be calculated by Eq. (6):

$$\begin{array}{ll} \text{Mode I strain energy release rate} & \text{Mode II strain energy release rate} \\ G_I = \frac{K_I^2}{E_I} & G_{II} = \frac{K_{II}^2}{E_{II}} \end{array} \quad (6)$$

where E_I and E_{II} are effective moduli for orthotropic materials. In order to apply the linear elastic fracture mechanics, the test sample must have some conditions. One of these is a load-displacement curve of the cracked test sample, which must show the linear elastic material behavior. Another requirement is that the strain state in the crack tip is known. When a material with a crack is loaded in tension, the materials develop plastic strains as the yield stress is exceeded in the region near the crack tip. Material within the crack tip stress field, situated close to a free surface, can deform laterally because there can be no stresses normal to the free surface. The state of stress tends to biaxial, and the material fractures in a characteristic ductile manner, with a 45° shear lip being formed at each free surface. This condition is called “plane stress,” and it occurs in relatively thin bodies where the stress through the thickness cannot vary appreciably due to the thin section. Knitted fabric-reinforced composite materials conform to the conditions of thin plates. Therefore, the plane stress state occurs at the crack tip. E_I and E_{II} according to the plane stress state are expressed in Eq. (7) [32, 37]:

$$E_I = \frac{\sqrt{2E_w E_c}}{\sqrt{\sqrt{\frac{E_w}{E_c}} + \frac{2\theta G_{wc} + E_w}{2G_{wc}}}}, E_{II} = \frac{\sqrt{2E_w}}{\sqrt{\sqrt{\frac{E_w}{E_c}} + \frac{2\theta G_{wc} + E_w}{2G_{wc}}}} \quad (7)$$

where E_w is elasticity modulus in the wale direction and E_c is elasticity modulus in the course direction. In order to determine the mixed-mode strain energy release rate value, Eq. (8) is utilized [32]:

$$G_C = G_I + G_{II} \quad (8)$$

where similar to the effective fracture toughness formula, the values of G_I and G_{II} represent the energy release values in mode I and mode II directions.

4. Finite element analysis

In fracture analysis of composite materials, J-integral method expresses the stress energy release rate or work (energy) per unit fracture surface area. The J-integral defines the plastic stress and strain intensity in a manner similar to the fracture toughness (K) parameter, which represents the stress intensity of the surrounding elastic field, in the crack vicinity. The J-integral depends on stress, strain, crack size, and the geometry of the crack and body. The expression of J in the 2D form can be given by Eq. (9). It assumes that the crack lies in the global Cartesian x(u)–y(v) plane:

$$J = \int_{\Gamma} \left(W n_i^e - n_i^e \sigma_{ij} \frac{\partial u_j}{\partial x_1} \right) d\Gamma_e \quad (9)$$

where Γ is a contour around the crack in the Cartesian coordinate system, W is stress field energy density, and x_i , u_i , and σ_{ij} are the spatial coordinates, the displacements, and the Cauchy stresses, respectively. n_i^ϵ are the components of the unit outward normal vector on Γ_ϵ . The coordinate system and typical J-integral paths were illustrated in **Figure 4**. For a linearly elastic solid, the strain energy density is expressed in Eq. 10:

$$W = W(x, \epsilon) = \frac{1}{2} \sigma_{ij} \epsilon_{ij} = \frac{1}{2} E_{ijkl}(x) \epsilon_{ij} \epsilon_{kl} \quad (10)$$

where $E_{ijkl}(x)$ are the Cartesian components of the fourth-order tensor expressing the generalized Hooke's law, ϵ is the strain tensor, and ϵ_{ij} are its Cartesian components [38]. Notice that the line integral shown in **Figure 4** is evaluated in a counterclockwise direction beginning on the lower crack surface and ending on the upper crack surface. The J-integral approach is a measure of the energy release rate associated with crack onset. One of the advantages of using J-integral is that under quasi-static conditions, it is equal to the energy release rate G for linear elastic materials [39]. Assuming linear elastic conditions prevailing along the integration path Γ , the numerical value of the J-integral can be related to the fracture toughness in plane stress condition as in Eq. (11) [40]:

$$J = \frac{K_C^2}{E} \quad (11)$$

The numerical analysis was performed in the commercial finite element software ANSYS Workbench by the use of a quasi-static rate-independent J-integral method, which can be used to determine the pure mode and mixed-mode fracture toughness. Eight-node quadrilateral plane elements with two degrees of freedom per node were used to model the cracked test specimens. The element has plasticity, creep, swelling, stress stiffening, large deflection, and large strain capabilities. The mesh was refined around the crack tip so that the smallest element size found in the crack tip elements was approximately 0.2 mm. The numerical model consists of 29,600 nodes approximately. An implicit solver was used for the finite element analysis. Implicit solutions are based on quantities calculated in the previous time step (backward Euler time scheme), which means even for large time steps the solution remains stable (unconditionally stable) [41]. In modeling fracture mechanics for laminated composite where both tensile and shear failure are common, a fracture criterion for predicting mode I, mode II, and mixed-mode I/II fracture onset is needed. Crack tip opening displacement test or CTOD is one of a

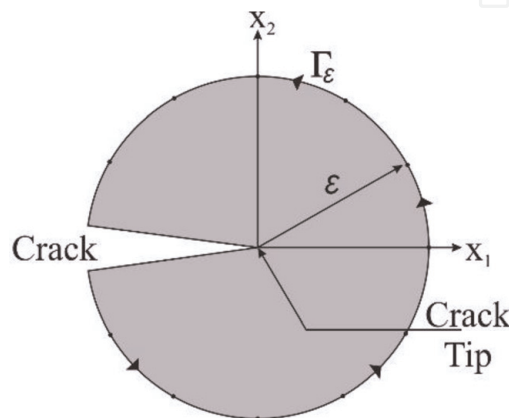


Figure 4.
The coordinates and typical paths to evaluate the J-integral.

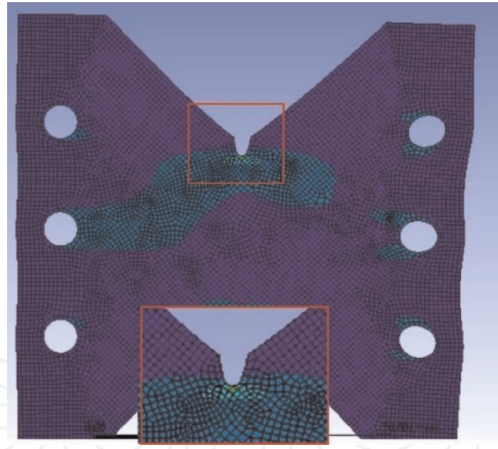


Figure 5.
The state of the finite element model after the analysis.

family of fracture criteria that measures the resistance of a material to growing a crack. In this context, CTOD failure criteria were employed for the crack onset in finite element analysis. There are two elastic-plastic parameters widely accepted by the fractured community; J-integral and CTOD [42, 43]. In case of LEFM, the elastic calculation for the CTOD can be expressed in Eq. (12):

$$\text{CTOD} = \frac{4}{\pi} \frac{K}{E \sigma_{ys}} \quad (12)$$

where K is the stress intensity factor, E is the effective modulus, and σ_{ys} is the uniaxial yield stress of the composite material.

The connection between the fixture and specimen is idealized by a rigid and continuous joint, based on the fact that the fixture and pins used in Arcan tests are relatively rigid compared to the specimen. Thus in the finite element analysis, the specimen-fixture system was treated as one continuous solid with two regions of different thickness and material properties. The fixed boundary condition was used, and distributed loads were assigned for the numerical model. **Figure 5** shows the state of the finite element model after the analysis.

5. Results and discussion

5.1 Results of Arcan fracture toughness test

The fracture tests were carried out using the Arcan test apparatus for 0°, 30°, 45°, 60°, and 90° loading angles. **Figure 6** has presented the load-displacement curve of pure glass/epoxy and pure carbon/epoxy at different loading angles. Load-displacement graphs of hybrid composites are not given because they behave similarly to others. When the loading angle changes from mode I to mode II plane, the maximum damage load (P_C) has increased. In addition, when the loading angle increased, specimens showed more deformation under load due to the increasing shear tendency of the test specimens. The fracture test was repeated five times for pure mode I (0°), pure mode II (90°), and all mixed-mode (30°, 45°, and 60°), and the obtained average P_C values are given in **Table 2**.

The average P_C values of critical fracture loads were used to determine the fracture toughness (K) and strain energy release rates (G) for all fracture modes. Calculated fracture toughness K_I , K_{II} , and K_{eff} according to the crack side was given in **Tables 3** and **4**, respectively.

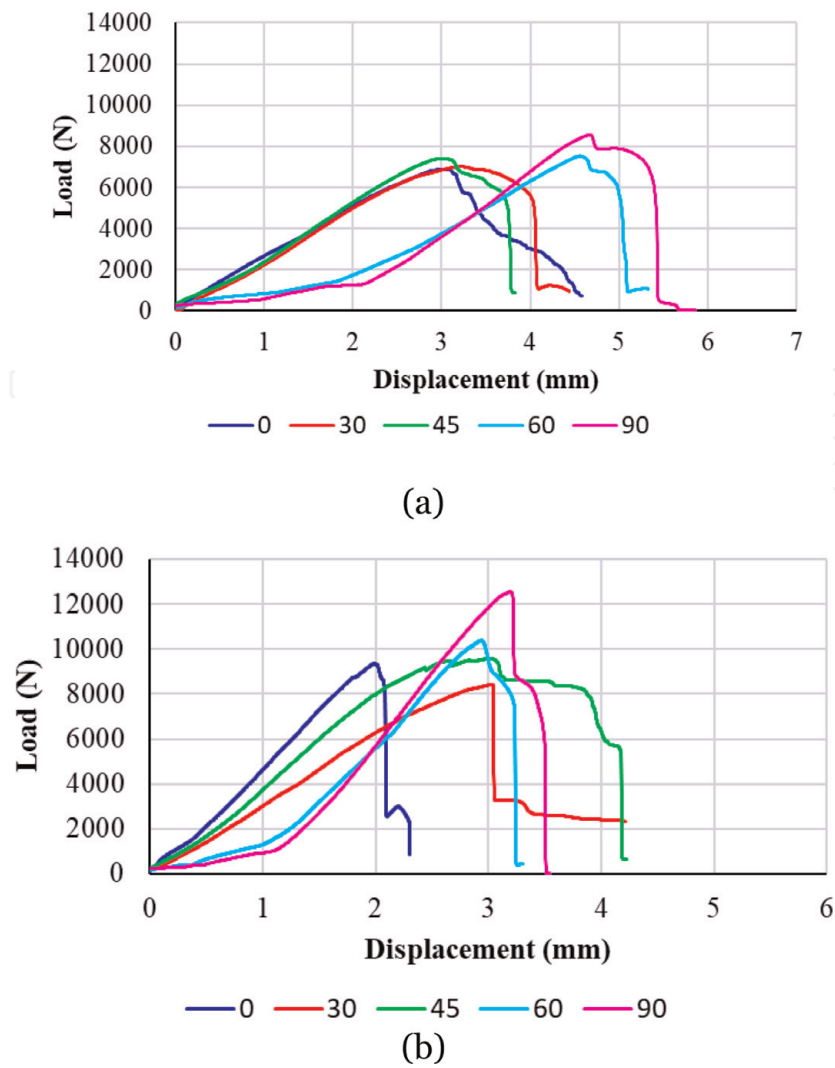


Figure 6. Load-displacement curves according to loading angles (a) pure glass/epoxy and (b) pure carbon/epoxy.

Material type		Loading angle				
		0°	30°	45°	60°	90°
Glass side cracked	Pure glass/epoxy	6883	6902	6453	7576	8553
	Carbon-glass/epoxy (12.5 mm width)	8642	7970	8557	9345	9669
	Carbon-glass/epoxy (25 mm width)	8531	7791	8323	8990	8917
	Carbon-glass/epoxy (50 mm width)	7900	7373	7440	8405	8745
Carbon side cracked	Pure carbon/epoxy	9358	8406	9567	10366	12510
	Carbon-glass/epoxy (12.5 mm width)	8771	8772	9119	9816	9943
	Carbon-glass/epoxy (25 mm width)	8718	8187	9049	9453	9654
	Carbon-glass/epoxy (50 mm width)	8426	8178	8491	9356	9413

Table 2. Average critical fracture loads P_C (N) for pure and hybrid knitted fabric laminated composites.

The calculated fracture toughness results showed that the loading angle, crack position, and pattern width directly affect the fracture behavior of the composite material. As loading angle increases from mode I to mode II, fracture toughness for each material type decreases. Applied load during mode I loading case forces the crack to open. So, damage occurs in the form of fiber and matrix fracture. In the

Material type		Loading angle				
		0°	30°	45°	60°	90°
Pure glass/epoxy	K_I	562.55	441.17	343.75	259.71	–
	K_{II}	–	63.46	83.40	109.18	161.30
	K_{eff}	562.55	445.71	353.72	281.73	161.30
Carbon-glass/epoxy (12.5 mm)	K_I	629.80	500.37	438.25	336.11	–
	K_{II}	–	70.28	110.97	146.10	158.59
	K_{eff}	629.80	505.28	452.08	366.50	158.59
Carbon-glass/epoxy (25 mm)	K_I	597.71	468.11	398.30	330.30	–
	K_{II}	–	67.03	103.33	135.53	146.70
	K_{eff}	597.71	472.89	411.49	357.02	146.70
Carbon-glass/epoxy (50 mm)	K_I	585.46	454.56	383.10	304.46	–
	K_{II}	–	64.14	94.61	130.11	141.90
	K_{eff}	585.46	459.06	394.61	331.10	141.90

Table 3.
Fracture toughness (MPa√mm) for carbon-glass/epoxy laminated composites with glass side cracked.

Material type		Loading angle				
		0°	30°	45°	60°	90°
Pure carbon/epoxy	K_I	664.64	532.40	494.83	360.78	–
	K_{II}	–	73.25	119.60	159.56	177.15
	K_{eff}	664.64	537.41	509.08	394.49	177.15
Carbon-glass/epoxy (12.5 mm)	K_I	635.60	523.76	467.58	352.70	–
	K_{II}	–	71.40	115.39	153.05	165.03
	K_{eff}	635.60	528.60	481.61	384.47	165.03
Carbon-glass/epoxy (25 mm)	K_I	619.57	505.11	436.68	345.04	–
	K_{II}	–	70.15	109.41	147.50	151.22
	K_{eff}	619.57	509.96	450.18	375.24	151.22
Carbon-glass/epoxy (50 mm)	K_I	599.85	479.02	415.84	337.96	–
	K_{II}	–	68.60	107.79	144.49	148.98
	K_{eff}	599.85	483.90	429.59	367.55	148.98

Table 4.
Fracture toughness (MPa√mm) for carbon-glass/epoxy laminated composites with carbon side cracked.

case of the opening mode, the damage occurs in the form of a matrix crack and subsequent fiber breakage. Also, the breakage occurs in a fast and brittle form, due to high-stress concentrations occurring at the crack end in the opening mode. During mode II loading, the applied load progresses the crack by shearing. As a result of shear deformation, the separation between laminas named delamination occurs. Damage of the brittle matrix material holding the lamina together allows the delamination to spread easily between the laminas. Thus, the material gains more ability to deform. The loads on the sample are transferred to the reinforcing hybrid fabric with increasing deformation, and the fiber structure is subjected to shear force. Due to the anisotropic behavior of the knitting structure, it can be seen from

fracture test results that the shear strength of reinforcement fabric was higher than the tensile strength.

When fracture toughness values of pure glass and carbon fabric-reinforced composites were compared, fracture toughness of carbon/epoxy composites was found to be up to 43% higher than glass/epoxy. If a similar comparison is made for hybrid composites that had the same pattern width, the fracture toughness of the samples with carbon side cracked is 11% higher than for samples with glass side cracked. According to the results obtained from pure and hybrid composites, the crack on the carbon side has a tougher spreading mechanism than on the glass side.

Although all hybrid fabric-reinforced composites contain equal amounts of glass and carbon fiber, different fracture toughness values were obtained for the same loading angle and crack location. Glass and carbon knitting pattern widths of hybrid fabrics have affected the fracture toughness of the material. At the combination boundary of the glass and carbon fiber knitting, a new intermediate form is occurred by the interlocking of glass fiber and carbon fiber loops. This intermediate form increased the strength of the structure due to exhibited behavior that is as flexible as the glass fiber and as strong as the carbon fiber. Accordingly, the fracture toughness value of the material has increased by decreasing pattern width or in other words increasing the number of intermediate forms. When the fracture toughness values at the same loading angle of the samples having the carbon side crack were compared with regard to the pattern width, the samples having a pattern width of 12.5 mm have more toughness value up to 9 and 12%, respectively, than the samples with 25 and 50 mm pattern width. If the similar comparison was made for the samples having a crack on the glass side, it was seen that the samples with a pattern width of 12.5 mm have more toughness value up to 10 and 15% than those with a pattern width of 25 and 50 mm, respectively.

5.2 Results of finite element analysis

A numerical study was also performed by using ANSYS finite element program for all loading angles. Some mechanical test values, which required to create a finite element model of glass and carbon knitted fabric-reinforced composite structures, were determined experimentally, and the obtained results are given in **Table 5**. The elasticity modulus in the wale direction (E_w) and the course direction (E_c) and the tensile strength in the wale (T_w) and course direction (T_c) of laminated composites were determined according to ASTM D3039M standard [44]. Shear modulus (G_{wc}) was determined according to the ASTM D3518M-13 standard test method [45]. Compressive properties were determined according to the ASTM D3410-87 standard test method [46]. Wale and course direction compressive strength of composite specimens (C_w and C_c) were calculated by dividing the failure load to the cross-sectional area of the specimens in wale and course direction, respectively. The in-plane shear properties in the wale direction (S_{wc}) and in the course direction

Material type	E_w (MPa)	E_c (MPa)	G_{wc} (MPa)	T_w (MPa)	T_c (MPa)	C_w (MPa)	C_c (MPa)	S_{wc} (MPa)	S_{cw} (MPa)
Glass/epoxy	24105.84	19621.19	4160.16	127.82	117.80	98.61	81.94	40.33	36.21
Carbon/epoxy	40437.71	29891.17	5112.89	200.91	156.36	125.80	99.27	51.94	46.23

Table 5.
Mechanical properties of nonhybrid knitted fabric-reinforced composite specimens.

Material type		Loading angle				
		0°	30°	45°	60°	90°
Pure glass/epoxy	J_{int}	17.81	8.52	3.19	2.16	1.28
	G_c	14.98	9.38	5.88	3.68	1.06
Carbon-glass/epoxy (12.5 mm)	J_{int}	16.97	11.61	9.63	6.65	0.95
	G_c	18.78	12.05	9.59	6.22	1.02
Carbon-glass/epoxy (25 mm)	J_{int}	14.93	11.13	7.93	5.53	0.90
	G_c	16.91	10.56	7.94	5.91	0.88
Carbon-glass/epoxy (50 mm)	J_{int}	14.34	10.02	7.93	4.82	0.67
	G_c	16.23	9.95	7.31	5.08	0.82

Table 6.
Comparison of J-integral and strain energy release rate (G_c) of glass side cracked specimens.

(S_{cw}) of glass and carbon knitted fabric-reinforced composites were determined according to ASTM D 5379 standard by using V-notched test samples [47]. The S_w and S_c have been found by dividing of maximum load by the cross-sectional area of the samples. All the tests for the mechanical properties were done five times for each material structure in room temperature. The average results of these five tests were accepted as mechanical property values. When **Table 5** is investigated, it can be seen that the mechanical strength of carbon/epoxy composite is higher than the glass/epoxy composite. Such that, tensile properties of pure carbon/epoxy as E_w , E_c , T_w , and T_c are 67.75, 52.34, 57.18, and 32.73% higher than glass/epoxy, respectively. The compression strength of carbon/epoxy in wale and course direction are 27.57 and 21.15% higher than glass/epoxy, respectively. For the comparison of shear modulus and shear strength, it can be seen that G_{wc} , S_{wc} , and S_{cw} values of carbon/epoxy are 22.9, 28.78, and 27.66% higher than glass/epoxy, respectively.

From the physical point of view, the energy release rate is the most appropriate physical quantity to characterize the fracture behavior. For purely elastic materials, the energy release rate G is identical to the J-integral because there is no energy stored in the crack cavity. In linear elastic fracture mechanics, the J-integral coincides with total energy release rate, $J_{int} = G_c = G_I + G_{II} + G_{III}$, where G_I , G_{II} , and G_{III} are the energy release rates associated with the mode I, mode II, and mode III stress intensity factors. In this study, the energy release rate (G) is obtained by using experimental data in theoretical formulas.

The J-integral value is calculated by the ANSYS program with the aid of the finite element model. The comparisons of the J-integral and strain energy release rate values, which were obtained from experimental and numerical analyses, were given in **Tables 6** and **7** depending on the crack location. When the comparisons in **Tables 6** and **7** are examined, it is seen that experimental and numerical results are compatible with each other. However, for the samples having the same pattern width, the energy required to progress the carbon side crack is higher than the glass side crack at the same loading angle.

In linear elastic fracture mechanics, Eq. (11) is valid between the fracture stress intensity factor (K_C) and the J-integral value for plane stress and plane strain cases. During the analysis, if the thickness of the material is neglected, plane stress condition is applicable, and if it is included in the solution, the plane strain condition is applicable. Depending on the J-integral value obtained from finite element numerical analysis, fracture toughness was determined according to Eq. 13 for plane stress condition [30, 37, 48]:

$$K_J = \sqrt{J.E_{effective}}$$

(13)

A comparison of the experimentally obtained fracture toughness values ((K_C)_{exp}) and the numerical fracture toughness values obtained using J-integral ((K_J)_{num}) is given in **Tables 8** and **9** according to the crack location.

According to **Tables 8** and **9**, it can be said that the results are close to each other when numerical values are compared with experimental values. The maximum error value was 15% for the finite element analysis when the experimental values are taken as reference. This maximum error value indicates that the numerical model created for finite element analysis successfully converges to the fracture test condition.

Damage modes and stress distributions of laminated composites were given in **Figure 7** after experimental fracture damage and FEM analysis. Due to important stress concentrations around the notches in uniaxial tension, specimen fracture

Material type		Loading angle				
		0°	30°	45°	60°	90°
Pure carbon/epoxy	J_{int}	18.38	11.98	9.81	6.65	1.47
	G_c	20.91	13.64	12.17	7.20	1.28
Carbon-glass/epoxy (12.5 mm)	J_{int}	17.45	12.96	9.82	7.09	1.09
	G_c	19.12	13.19	10.89	6.84	1.11
Carbon-glass/epoxy (25 mm)	J_{int}	15.20	11.05	8.84	5.84	0.95
	G_c	18.17	12.28	9.51	6.52	0.93
Carbon-glass/epoxy (50 mm)	J_{int}	15.62	10.26	7.82	5.52	1.05
	G_c	17.03	11.05	8.66	6.26	0.90

Table 7.
Comparison of J-integral and strain energy release rate (G_c) of carbon side cracked specimens.

Material type		Loading angle				
		0°	30°	45°	60°	90°
Pure glass/epoxy	(K_C) _{exp}	562.55	445.71	353.72	281.73	161.30
	(K_J) _{num}	516.85	417.70	317.40	261.29	145.66
	% error	8.12	6.28	10.27	7.25	9.70
Carbon-glass/epoxy (12.5 mm)	(K_C) _{exp}	629.80	505.28	452.08	366.50	158.59
	(K_J) _{num}	639.68	551.30	515.75	400.53	172.45
	% error	1.57	9.11	14.08	9.29	8.74
Carbon-glass/epoxy (25 mm)	(K_C) _{exp}	597.71	472.89	411.49	357.02	146.70
	(K_J) _{num}	549.63	536.17	462.49	371.52	159.11
	% error	8.04	13.38	12.39	4.06	8.46
Carbon-glass/epoxy (50 mm)	(K_C) _{exp}	585.46	459.06	394.61	331.10	141.90
	(K_J) _{num}	499.28	517.96	437.08	377.01	127.37
	% error	14.72	12.83	10.76	13.87	10.24

Table 8.
Experimental and numerical fracture toughness values of glass side cracked specimens.

Material type		Loading angle				
		0°	30°	45°	60°	90°
Pure glass/epoxy	$(K_C)_{exp}$	664.64	537.41	509.08	394.49	177.15
	$(K_f)_{num}$	623.11	564.88	468.68	408.48	189.78
	% error	6.25	5.11	7.94	3.55	7.13
Carbon-glass/epoxy (12.5 mm)	$(K_C)_{exp}$	635.60	528.60	481.61	384.47	165.03
	$(K_f)_{num}$	607.15	597.83	541.68	426.50	180.12
	% error	4.48	13.10	12.47	10.93	9.14
Carbon-glass/epoxy (25 mm)	$(K_C)_{exp}$	619.57	509.96	450.18	375.24	151.22
	$(K_f)_{num}$	674.09	574.84	513.97	417.84	163.68
	% error	8.80	12.72	14.17	11.35	8.24
Carbon-glass/epoxy (50 mm)	$(K_C)_{exp}$	599.85	483.90	429.59	367.55	148.98
	$(K_f)_{num}$	524.25	553.78	484.21	406.19	160.65
	% error	12.60	14.44	12.72	10.51	7.83

Table 9.
Experimental and numerical fracture toughness values of carbon side cracked specimens.

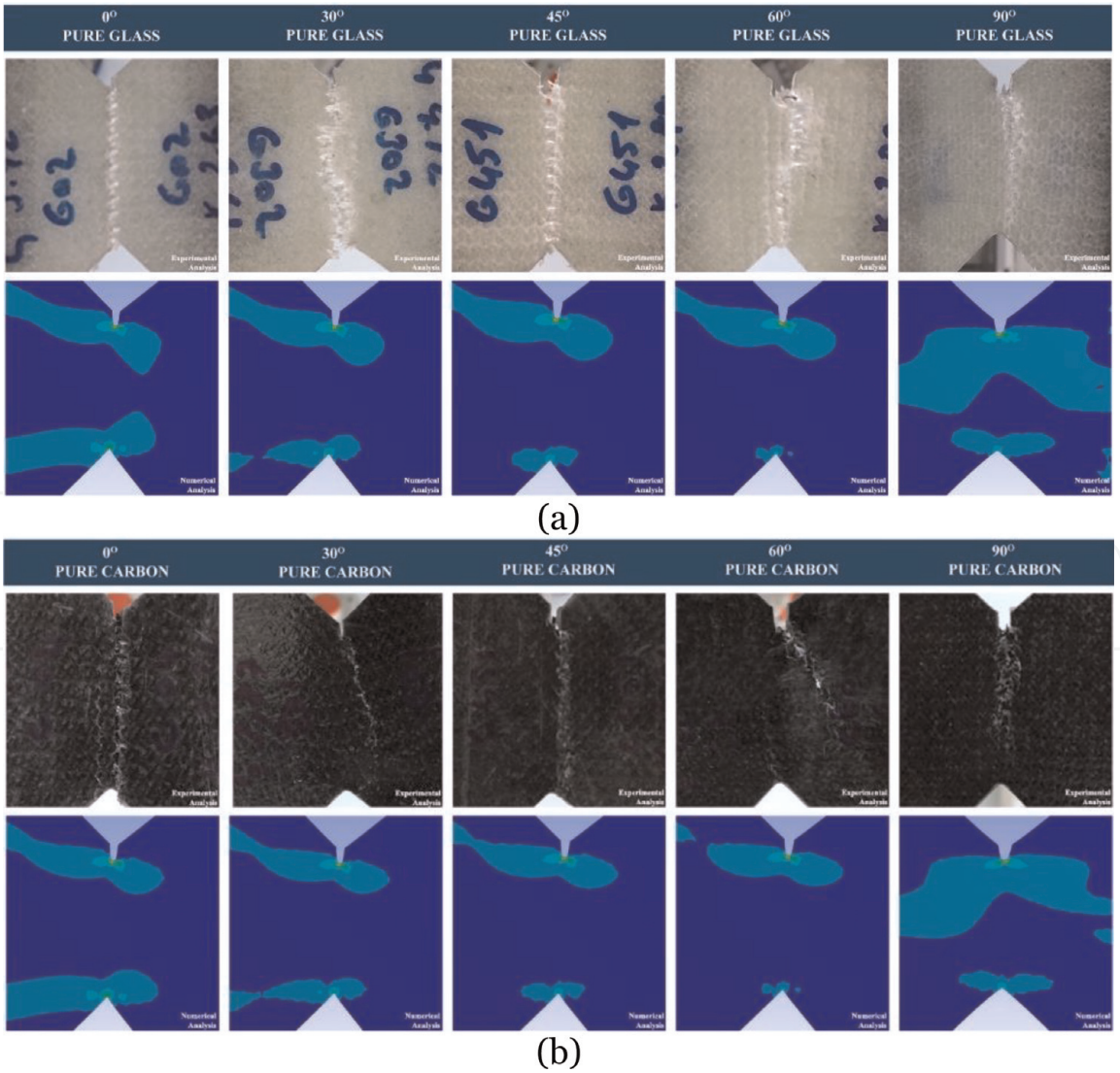


Figure 7.
Damage and stress distributions after experimental fracture and FEM analysis of laminated composites for (a) glass/epoxy and (b) carbon/epoxy.

generally occurred in the significant crack tip. As noticed from previous tests, the fracture mechanism consisted of one unique cracked interface identical for all glass/epoxy composite samples tested whatever the loading direction. In such a case, the crack propagated between the two loops of rows, which is in the direction of the wale, and the crack could not pass through the other loops. Although different crack onset mechanisms did not appear depending on the loading angle in the glass/epoxy specimens, FEM analyses have shown that the stress distributions in the crack region vary depending on the loading angle. Fractured carbon/epoxy composite samples presented a nearly horizontal cracked zone that was different from a plane surface for loading angle of 30° and 60°. During the experimental Arcan test, it was observed that the crack progress in the main delamination plane without any side cracking and branching. Fiber bending and breaking behind the crack tip were observed macroscopically in crack onset during the test.

The experimental and numerical analysis visual results of hybrid composites with 12.5 mm pattern width, which have the maximum fracture toughness values, are given in **Figure 8**. The crack propagates by the glass in **Figure 8(a)** and by carbon in **Figure 8(b)**. Von Mises stress distribution for different loading angles, which obtained from finite element analysis, is shown. The crack started from the

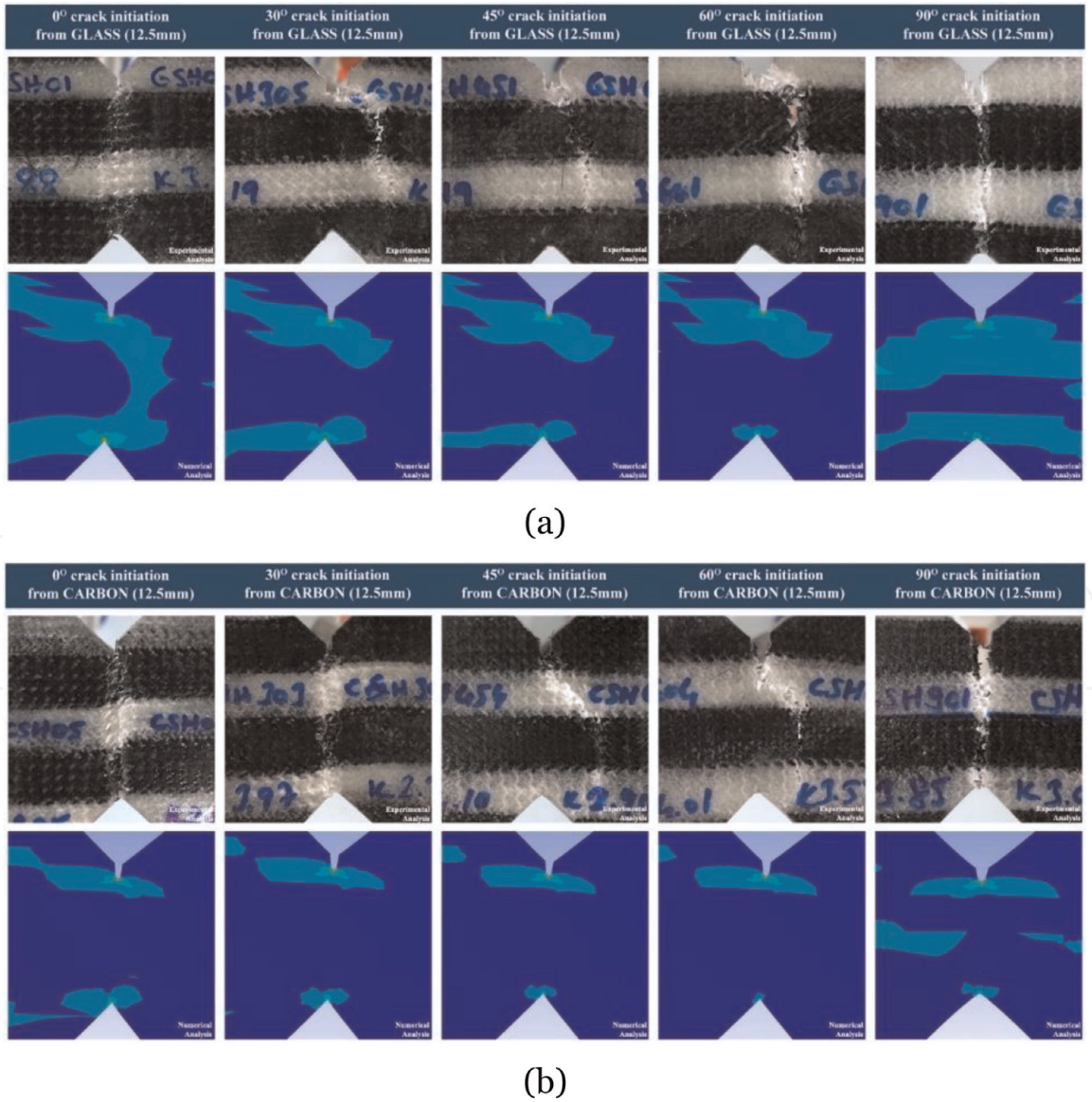


Figure 8.
The experimental and numerical visual results of hybrid composites with 12.5 mm pattern width having (a) glass side crack and (b) carbon side crack.

crack tip due to high-stress concentration at the crack tip, and it propagates to the other side by breaking fibers and/or fiber pull out. It can be clearly said that the numerical damage forms were obtained in the similar views of the experimental damage forms as illustrated in **Figure 8**. According to the results of numerical damage, Von Mises stresses show a vertical progression in the case of mode I, while a more horizontal progression occurs in the case of mode II.

6. Conclusion

This paper has presented the fracture behavior of pure and hybrid knitted fabric-reinforced laminated composites based on experimental and numerical analyses. In this context, the effect of crack location, loading angle, and pattern width on fracture behavior are examined. A modified version of the Arcan test fixture was employed to conduct a mode I, mode II, and mode I/II test. The obtained fracture test results of hybrid specimens are compared with the test results of pure glass/epoxy and pure carbon/epoxy samples. In addition, finite element models of cracked test specimens were created according to the data obtained from the mechanical tests. Fracture behaviors of hybrid composites were numerically analyzed using J-integral method. The concluding remarks in this study can be summarized as follow:

- According to the results obtained from the mechanical tests, knitted fabrics have been found to be an alternative to woven fabrics for reinforcing polymer composites. In addition, the test results show that the mechanical strength values change depending on the knitting direction and all mechanical test values are larger in the wale direction.
- The maximum and minimum fracture toughness value for carbon-glass/epoxy hybrid laminated composites was obtained in mode I and mode II loading conditions. The highly complex structure of the knitted fabric composites induces various toughening mechanisms. Fracture toughness behaviors of pure and hybrid composites varied in terms of loading angle. When, the loading angle increased from 0 (mode I) to 90 (mode II), the critical damage load increases. On the contrary, the fracture toughness and energy release rate decreases. The results indicated that the Arcan cracked specimen is tougher in tensile loading conditions and weaker in shear loading conditions.
- The rib-knitted fabric-reinforced composite shows different fracture toughness and energy release rate values for both crack progression directions despite the fact that damage images showed that the crack growth modes are different: in the wale direction, the crack followed the wavy surface of the fabric, and in the course direction, the majority of yarns is broken. In the wale direction, the major fracture mechanisms were the matrix deformations, leading to micro-cracks, which will branch in a network. In the course direction, the crack does not strictly follow the waviness of the fabrics but tends to grow through them. The main damage occurs by multiple fiber breakage. This phenomenon is supposed to be highly energy consuming because it implies events such as peel off, yarn bridging, and yarn failure.
- For all fracture tests of pure fabric-reinforced composite, carbon/epoxy specimens were much more resistant than glass/epoxy in terms of failure loads whatever the loading angle.

- As the width of the pattern increased, the fracture strength of the hybrid composites decreased. In this respect, the hybridization processing should be done in the narrowest pattern width for high resistance to fracture.
- In terms of crack locations, the progression of the crack in the glass-reinforced zone is more hazardous than the progress in the carbon reinforcing zone. During the assembly of carbon-glass hybrid composites, it is better to ensure that the bolt holes are opened on the carbon side if the bolts are to be used.
- When the fracture toughness values that were obtained experimentally and numerically are compared, it is seen that the results are consistent. In addition, in terms of fracture energy, experimentally obtained strain energy release rate (G) and numerical fracture energy (J-integral) values are similar. In this respect, the usability and validity of the J-integral method have been proven to simulate numerical fracture analysis of knitted fabric-reinforced laminated composites.

Author details


Huseyin Ersen Balcioglu^{1*} and Hayri Baytan Ozmen²

1 Department of Mechanical Engineering, Usak University, Usak, Turkey

2 Department of Civil Engineering, Usak University, Usak, Turkey

*Address all correspondence to: ersen.balcioglu@usak.edu.tr

IntechOpen

© 2019 The Author(s). Licensee IntechOpen. This chapter is distributed under the terms of the Creative Commons Attribution License (<http://creativecommons.org/licenses/by/3.0>), which permits unrestricted use, distribution, and reproduction in any medium, provided the original work is properly cited. 

References

- [1] Balcioğlu HE, Sakin R, Gün H. The design of multi-sample flexural fatigue device and fatigue behavior of glass/epoxy laminated composites. *Research on Engineering Structures and Materials*. 2018;**4**:279-296. DOI: 10.17515/resm2018.67me0917
- [2] Atay HY. Multi-functional materials for military aircrafts; radar absorbing and flame retardant composites. *Research on Engineering Structures and Materials*. 2016;**3**:45-54. DOI: 10.17515/resm2016.38ma0204
- [3] Costa DMS, Loja MAR. On the characterization of the free vibrations behavior of multiscale composite plates. *Research on Engineering Structures and Materials*. 2016;**3**:27-44. DOI: 10.17515/resm2016.43st0602
- [4] Karakoç A. A fiber network model to understand the effects of fiber length and height on the deformation of fibrous materials. *Research on Engineering Structures and Materials*. 2016;**2**:51-57. DOI: 10.17515/resm2015.17ma0825
- [5] Ashraf W, Nawab Y, Umair M, Shaker K, Karahan M. Investigation of mechanical behavior of woven/knitted hybrid composites. *Journal of the Textile Institute*. 2017;**108**:1510-1517. DOI: 10.1080/00405000.2016.1258951
- [6] Nesrin Sahbaz K, Yekta K, Huseyin O, Gokce O. Textile reinforced structural composites for advanced applications. *Textiles for Advanced Applications*. 2016;**13**. DOI: 10.5772/intechopen.68245
- [7] Muralidhar BA. Tensile and compressive behaviour of multilayer flax-rib knitted preform reinforced epoxy composites. *Materials and Design*. 2013;**49**:400-405. DOI: 10.1016/j.matdes.2012.12.040
- [8] Pei X, Shang B, Chen L, Li J, Tang Y. Compression properties of multilayer-connected biaxial weft knitted carbon fiber fabric reinforced composites. *Composites. Part B, Engineering*. 2016;**91**:296-305. DOI: 10.1016/j.compositesb.2015.12.041
- [9] Kim KY, Curiskis JI, Ye L, Fu SY. Mode-I interlaminar fracture behaviour of weft-knitted fabric reinforced composites. *Composites. Part A, Applied Science and Manufacturing*. 2005;**36**:954-964. DOI: 10.1016/j.compositesa.2004.12.004
- [10] Falconnet D, Bourban PE, Pandita S, Manson JAE, Verpoest I. Fracture toughness of weft-knitted fabric composites. *Composites. Part B, Engineering*. 2002;**33**:579-588. DOI: 10.1016/S1359-8368(02)00053-7
- [11] Dadej K, Bienias J, Surowska B. On the effect of glass and carbon fiber hybridization in fiber metal laminates: Analytical, numerical and experimental investigation. *Composite Structures*. 2019;**220**:250-260. DOI: 10.1016/j.compstruct.2019.03.051
- [12] Tabrizi IE, Kefal A, Zanjani JSM, Akalin C, Yildiz M. Experimental and numerical investigation on fracture behavior of glass/carbon fiber hybrid composites using acoustic emission method and refined zigzag theory. *Composite Structures*. 2019;**223**:110971. DOI: 10.1016/j.compstruct.2019.110971
- [13] Swolfs Y, Gorbatiikh L, Verpoest I. Fibre hybridisation in polymer composites: A review. *Composites. Part A, Applied Science and Manufacturing*. 2014;**67**:181-200. DOI: 10.1016/j.compositesa.2014.08.027
- [14] Wisnom MR, Czél G, Swolfs Y, Jalalvand M, Gorbatiikh L, Verpoest I. Hybrid effects in thin ply carbon/glass

- unidirectional laminates: Accurate experimental determination and prediction. *Composites. Part A, Applied Science and Manufacturing*. 2016;**88**: 131-139. DOI: 10.1016/j.compositesa.2016.04.014
- [15] Dong C, Davies IJ. Flexural and tensile strengths of unidirectional hybrid epoxy composites reinforced by S-2 glass and T700S carbon fibres. *Materials and Design*. 2014;**54**:955-966. DOI: 10.1016/j.matdes.2013.08.087
- [16] Naito K, Oguma H. Tensile properties of novel carbon/glass hybrid thermoplastic composite rods. *Composite Structures*. 2017;**161**:23-31. DOI: 10.1016/j.compstruct.2016.11.042
- [17] Greenhalgh E, Hiley CM. The influence of fibre architecture in the failure of polymer composites. In: *Failure Analysis and Fractography of Polymer Composites*, Woodhead Publishing Series in Composites Science and Engineering. 2009. pp. 279-355. DOI: 10.1533/9781845696818.279
- [18] Zhao Y, Cao M, Lum WP, Tan VBC, Tay TE. Interlaminar fracture toughness of hybrid woven carbon-Dyneema composites. *Composites. Part A, Applied Science and Manufacturing*. 2018;**114**:377-387. DOI: 10.1016/j.compositesa.2018.08.035
- [19] Bieniaś J, Dadej K, Surowska B. Interlaminar fracture toughness of glass and carbon reinforced multidirectional fiber metal laminates. *Engineering Fracture Mechanics*. 2017;**175**:127-145. DOI: 10.1016/j.engfracmech.2017.02.007
- [20] Jung H, Kim Y. Mode I fracture toughness of carbon-glass/epoxy interply hybrid composites. *Journal of Mechanical Science and Technology*. 2015;**29**:1955-1962. DOI: 10.1007/s12206-015-0416-3
- [21] Saidane EH, Scida D, Pac MJ, Ayad R. Mode-I interlaminar fracture toughness of flax, glass and hybrid flax-glass fibre woven composites: Failure mechanism evaluation using acoustic emission analysis. *Polymer Testing*. 2019;**75**:246-253. DOI: 10.1016/j.polymertesting.2019.02.022
- [22] Swolfs Y, Geboes Y, Gorbatikh L, Pinho ST. The importance of translaminar fracture toughness for the penetration impact behaviour of woven carbon/glass hybrid composites. *Composites. Part A, Applied Science and Manufacturing*. 2017;**103**:1-8. DOI: 10.1016/j.compositesa.2017.09.009
- [23] Yeter E, Erklığ A, Bulut M. Hybridization effects on the buckling behavior of laminated composite plates. *Composite Structures*. 2014;**118**:19-27. DOI: 10.1016/j.compstruct.2014.07.020
- [24] Nisini E, Santulli C, Liverani A. Mechanical and impact characterization of hybrid composite laminates with carbon, basalt and flax fibres. *Composites. Part B, Engineering*. 2017;**127**:92-99. DOI: 10.1016/j.compositesb.2016.06.071
- [25] Bulut M, Erklığ A, Yeter E. Hybridization effects on quasi-static penetration resistance in fiber reinforced hybrid composite laminates. *Composites. Part B, Engineering*. 2016;**98**:9-22. DOI: 10.1016/j.compositesb.2016.05.025
- [26] ASTM International. ASTM D 5054 standard test methods for plane-strain fracture toughness and strain energy release rate of plastic materials. *ASTM B Stand*. 2013;**99**:1-9. DOI: 10.1520/D5045-14.priate
- [27] Khan Z, Yousif BF, Islam M. Fracture behaviour of bamboo fiber reinforced epoxy composites. *Composites. Part B, Engineering*. 2017;**116**:186-199. DOI: 10.1016/j.compositesb.2017.02.015
- [28] Silva RV, Spinelli D, Bose Filho WW, Claro Neto S, Chierice GO,

Tarpani JR. Fracture toughness of natural fibers/castor oil polyurethane composites. *Composites Science and Technology*. 2006;**66**:1328-1335. DOI: 10.1016/j.compscitech.2005.10.012

[29] Hanif WYW, Risby MS, Noor MM. Influence of carbon nanotube inclusion on the fracture toughness and ballistic resistance of twaron/epoxy composite panels. *Procedia Engineering*. 2015;**114**: 118-123. DOI: 10.1016/j.proeng.2015.08.049

[30] Kaman MO. Effect of fiber orientation on fracture toughness of laminated composite plates $[0^\circ/\theta^\circ]$ s. *Engineering Fracture Mechanics*. 2011;**78**:2521-2534. DOI: 10.1016/j.engfracmech.2011.06.005

[31] Arasan Ş, Aktaş M, Balcıoğlu HE. Fracture toughness of woven glass and carbon reinforced hybrid and non-hybrid composite plates. *Polymer Composites*. 2018;**39**:783-793. DOI: 10.1002/pc.23999

[32] Choupani N. Experimental and numerical investigation of the mixed-mode delamination in Arcan laminated specimens. *Materials Science and Engineering A*. 2008;**478**:229-242. DOI: 10.1016/j.msea.2007.05.103

[33] Hasanpour R, Choupani N. Rock fracture characterization using the modified Arcan test specimen. *International Journal of Rock Mechanics and Mining Sciences*. 2009;**46**:346-354. DOI: 10.1016/j.ijrmms.2008.07.004

[34] Yoon SH, Hong CS. Interlaminar fracture toughness of graphite/epoxy composite under mixed-mode deformations. *Experimental Mechanics*. 1990;**30**:234-239. DOI: 10.1007/BF02322816

[35] Jamali J, Mourad AHI, Fan Y, Wood JT. Through-thickness fracture behavior of unidirectional glass fibers/epoxy composites under various

in-plane loading using the CTS test. *Engineering Fracture Mechanics*. 2016;**156**:83-95. DOI: 10.1016/j.engfracmech.2016.01.016

[36] Jamali J, Fan Y, Wood JT. The mixed-mode fracture behavior of epoxy by the compact tension shear test. *International Journal of Adhesion and Adhesives*. 2015;**63**:79-86. DOI: 10.1016/j.ijadhadh.2015.08.006

[37] Nikbakht M, Choupani N. Numerical investigation of delamination in carbon-epoxy composite using arcan specimen. *International Journal of Mechanical and Mechatronics Engineering*. 2008;**2**:750-757

[38] Okada H, Kadowaki S, Suzuki M, Yusa Y. J-integral computation for elastic-plastic materials with spatially varying mechanical properties. *Engineering Fracture Mechanics*. 2019;**207**:181-202. DOI: 10.1016/j.engfracmech.2018.12.029

[39] Tafazzolimoghaddam B, Curiel-Sosa JL. On the calculation of energy release rates in composite laminates by finite elements, boundary elements and analytical methods. *Composites: Mechanics, Computations, Applications: An International Journal*. 2015;**6**: 219-237. DOI: 10.1615/CompMechComputApplIntJ.v6.i3.40

[40] González GLG, González JAO, Castro JTP, Freire JLF. A J-integral approach using digital image correlation for evaluating stress intensity factors in fatigue cracks with closure effects. *Theoretical and Applied Fracture Mechanics*. 2017;**90**:14-21. DOI: 10.1016/j.tafmec.2017.02.008

[41] Crump T, Ferté G, Jivkov A, Mummery P, Tran VX. Dynamic fracture analysis by explicit solid dynamics and implicit crack propagation. *International Journal of Solids and Structures*. 2017;**110-111**:

113-126. DOI: 10.1016/j.ijsolstr.2017.01.035

through thickness effects. International Journal of Fatigue. 2013;**46**:58-66. DOI: 10.1016/j.ijfatigue.2011.12.012

[42] Chabchoub M, Bouscarrat D, Vieille B, Gautrelet C, Beyaoui M, Taktak M, et al. Investigations on the mode I translaminar failure and determination of fracture toughness in woven-ply carbon fibers thermoplastic composites at high temperatures. Applied Acoustics. 2017;**128**:55-63. DOI: 10.1016/j.apacoust.2017.01.028

[43] Castrodeza EM, Perez Ipina JE, Bastian FL. Fracture toughness evaluation of unidirectional fibre metal laminates using traditional CTOD (δ) and Schwalbe (δ_5) methodologies. Engineering Fracture Mechanics. 2004; **71**:1107-1118. DOI: 10.1016/S0013-7944(03)00138-3

[44] ASTM International. Designation: D 3039/D 3039M–00 Standard Test Method for Tensile Properties of Polymer Matrix Composite Materials 1. 2002. p. 15. DOI: 10.1520/D3039_D3039M-08

[45] ASTM International. Designation: D 3518/D 3518M–94 Standard Test Method for In-Plane Shear Response of Polymer Matrix Composite Materials by Tensile Test of a $\pm 45^\circ$ Laminate. 2001;**5**: 1-7. DOI: 10.1520/D 3518/D_3518M-94

[46] ASTM International. ASTM-D3410 standard test method for compressive properties of polymer matrix composite materials with unsupported gage section by shear loading. Annual Book of ASTM Standards. 2003;**15**(03):1-16. DOI: 10.1520/D3410

[47] ASTM International. ASTM D5379: Standard Test Method for Shear Properties of Composite Materials by the V-Notched Beam Method. 1998. pp. 1-13

[48] Garcia-Manrique J, Camas D, Lopez-Crespo P, Gonzalez-Herrera A. Stress intensity factor analysis of